Kinetic energy distribution for photofission of light actinides

P. Mehdipour Kaldiani *
Department of Physics, Naragh Branch, Islamic Azad University, Naragh, Iran

(Received 22 June 2020; accepted 22 September 2020; published 14 October 2020)

The scission point model has been used to calculate the total kinetic energy (TKE) as a function of fission fragments for photofission reactions. By comparing the calculated TKE values with the available experimental data, the deformation parameters of the fission fragments are obtained in the scission point model. The results show that the deformation parameters of the fission fragments have a large change near the symmetrical region. TKE distribution has been investigated for neutron-induced fission, spontaneous fission, and photofission to predict actinide TKE distribution. This indicates that the TKE distribution depends on the mass and atomic number of compound nuclei and, of course, the excitation energy. The odd-even effect plays an important role in predicting TKE distribution behavior. Also, TKE distribution has a similar trend for all isotopes and the TKE distribution of spontaneous fission is significantly different from the TKE distribution of photofission. At last, the total kinetic energy distributions for the photofission fragments of light actinides are evaluated in the scission point model.

DOI: 10.1103/PhysRevC.102.044612

I. INTRODUCTION

During the 60 years that photofission and neutron-induced fission were discovered, the kinetic energy of fission fragments has been one of the important studies for understanding the fission process. The nuclear energy industry has made fissioning systems' actinides the main target of research. In addition, nuclear data on actinides have been used to manage nuclear waste and the Th-U cycle. Of course, the kinetic energy of fragments for neutron-induced fission [1–12] has been measured more than the kinetic energy of fragments for photofission [13–18]. In addition, there are the electromagnetic-induced fission [19] and spontaneous fission [20–24].

On the other hand, there is little theoretical work on TKE evaluation [25–33]. Each research group calculates TKE in one way: Manea *et al.* [26] refined the multimodal random neck rupture model, Pomorski *et al.* [29] used a quantum mechanical framework, and Usang *et al.* [28] described the dynamics of fission by Langevin's equations. Ivanyuk *et al.* [31,32] calculated deformation energy within the two-center shell-model parametrization and estimated the TKE of fission fragments in a quasistatic approximation. Andreev *et al.* [33] used a simple way to calculate the fine structures in the total kinetic energy of neutron-induced fission fragments using the scission point model. In this method, the scission configuration is expressed as a dinuclear system with the two fission fragments in contact. Also, Pasca *et al.* [25] changed the deformation parameter of each fission fragment to extract the potential energy. Ruben *et al.* [30] proposed a similar model called the two-spheroid model (TSM). The calculations of this systematic model have been compared with the experimental data in Ref. [13], in which the results of this model are in good agreement with the experimental results.

TSM model is a scission point model in which the scission configuration is assumed to consist of two spheroidally shaped fragments. In this model, two spheres are separated by a distance $d \approx 1.44$ fm [19,34], and the Coulomb repulsion energy between the two spheres, which are actually located effectively in the center of them, indicates the Coulomb energy of the system at the scission point.

Neutron-induced fission theoretical models are commonly used to calculate the total kinetic energy distribution for the photofission phenomenon, such as in the work of Pomme *et al.* [13], who used the TSM model. Here, the total kinetic energy distribution of actinides is studied for photofission phenomena. Therefore, the experimental results of TKE for neutron fission, photofission, and spontaneous fission are compared and investigated to estimate the best TKE values for the photofission phenomenon. Also, there are so few experimental results in the photofission phenomenon that there are no experimental results for fissioning nuclei with odd mass number. Thus, the TKE values for many actinides, especially odd nuclei, are evaluated in the photofission phenomenon.

The calculation framework is presented in Sec. II as the simplest model. In the next section, the calculated results are compared with the experimental data. Then, the total kinetic energy distribution (TKED) for neutron fission, spontaneous fission, and photofission is investigated to estimate the best result. At last, the total kinetic energy distribution is presented for the photofission of actinides. A brief summary is given in Sec. IV.

II. THEORETICAL FRAMEWORK

The total kinetic energy of the fission fragments is calculated with the simplest relation

*Payammehdipour@gmail.com

as [33]

$$TKE(A_i, \beta_i) = V_{\text{Coul}}(A_L/A_H, \beta_i, d) + V_{\text{nuc}}(A_L/A_H, \beta_i, d). \quad (1)$$

The deformation parameters of each fission fragment β_i is taken to be quadratic in the radius change (β_i; $i = L$ and H for the light and heavy fragments, respectively). The Coulomb interaction V_{Coul} is rewritten by taking quadrupole deformation alone and without taking orientation of the two fragments into account as [27,35]

$$V_{\text{Coul}} = \frac{Z_L Z_H e^2}{D}\left(1 + 0.3785\,\frac{R_2{}^2\beta_2 + R_1{}^2\beta_1}{D^2} + 0.3164\,\frac{R_1{}^2\beta_1{}^2 + R_2{}^2\beta_2{}^2}{D^2} + 0.20472\,\frac{R_1{}^4\beta_1{}^2 + R_2{}^4\beta_2{}^2}{D^4} + 0.8598\,\frac{R_1{}^2R_2{}^2\beta 1\,\beta 2}{D^4}\right), \quad (2)$$

where $D = d + R_1 + R_2$. The nuclear interaction between spherical fragments V_{nuc} is rewritten as the proximity potential [36,37]

$$V_{\text{prox}}(s) = 4\pi\gamma b\left[\frac{C_1C_2}{C_1 + C_2}\right]\Phi(\varepsilon), \qquad \left(\varepsilon = \frac{d}{b}\right), \quad (3)$$

where the width (diffuseness) of the nuclear surface is $b = 0.88$ fm. The nuclear surface tension coefficient of the nucleus γ is obtained from the Lysekil mass formula by [38]

$$\gamma = 0.9517\sqrt{\left(1 - 2.61I_1^2\right)\left(1 - 2.61I_2^2\right)} \quad \text{MeV/fm}^2,$$
$$I_i = \frac{(N_i - Z_i)}{A_i}, \quad (4)$$

where N_i, Z_i, and A_i are the neutron number, the atomic number, and the mass number of each fission fragment, respectively. C_1 and C_2 are the Süzmann central radii of light and heavy fragments that are related to the sharp radius R_i as

$$C_i = R_i - \left[\frac{b^2}{R_i}\right]. \quad (5)$$

R_i are the net radii of each fission fragment obtained through a semiempirical equation as [37]

$$R_i\,(\text{fm}) = 1.28R_{0,i} - 0.76 + 0.8R_{0,i}^{-1}. \quad (6)$$

$R_{0,i}$ are the radii of deformed nuclei that can be evaluated using the deformation-dependent expansion of nuclear radii as

$$R_{0,i}(\theta) = R_0\left[1 + \beta_{j,i}Y_{j0}(\theta)\right], \quad (7)$$

where θ is the angle made by the axis of symmetry with the fission axis and Y_{j0} are the spherical harmonic functions.

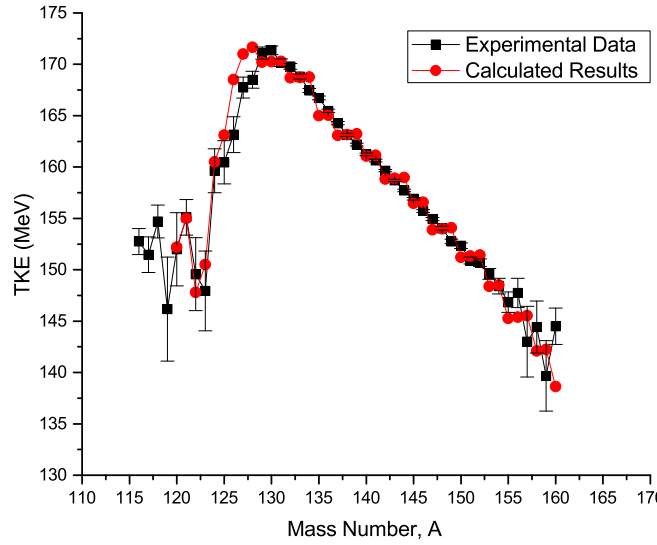

FIG. 1. Calculated total kinetic energy as a function of fragment mass at 9.5-MeV bremsstrahlung endpoint energy for photofission of ^{232}Th along with the experimental data [16].

In Eq. (3), the universal proximity potential Φ is a function of distance between two interaction fragments [36]:

$$\Phi(\varepsilon) = \begin{cases} -1.7817 + 0.9270\varepsilon + 0.0169\varepsilon^2 - 0.0514\varepsilon^3 \\ \quad \text{for} \quad 0 \leqslant \varepsilon \leqslant 1.9475, \\ -4.41\exp(-\varepsilon/0.7176) \\ \quad \text{for} \quad \varepsilon \geqslant 1.9475. \end{cases}$$

At last, for each mass number of fragments A_i, only one charge number Z_i was taken as the integer value of the most probable charge obtained from the common relation as [39]

$$Z_{\text{UCD}} = \frac{Z_{\text{cn}}\,(A_i + \nu)}{A_{\text{cn}}}, \quad (8)$$

where ν is the postscission neutrons [40,41].

III. RESULTS AND DISCUSSION

In Figs. 1–5 are presented the comparison of the calculated TKE values and the available experimental data as a function of fragment mass for photofission of ^{232}Th, ^{234}U, ^{238}U, ^{240}Pu, and ^{242}Pu, respectively. It is found that, when the mass number A of the fissioning nucleus increases, the deformation parameters of the fission fragments with mass number $A_i < 132$ must change. The deformation parameters for near symmetric fission fragments are presented in Table I for the mentioned fissioning nuclei using the scission point model. Here, the deformation parameters of two fission complementary fragments are considered equal to each other, so the sum of these two parameters is investigated and discussed. As Figs. 1–5 show, the obtained results indicate a good agreement between the calculated results and the experimental data when small variations in the deformation parameters are used, except for few fragments which have magic or semimagic neutron/proton numbers.

TABLE I. The change in $\beta_1 = \beta_2$ values of photofission of actinide for near fission fragments.

A_i	^{232}Th	^{234}U	^{238}U	^{240}Pu	^{242}Pu
120	0.88	0.59	0.76		0.84
121	0.8	0.57	0.88	0.84	0.84
122	1.0	0.56	0.56	0.78	0.78
123	0.9	0.49	0.63	0.77	0.78
124	0.65	0.57	0.68	0.75	0.75
125	0.63	0.5	0.51	0.71	0.68
126	0.58	0.45	0.5	0.67	0.67
127	0.468	0.5	0.435	0.63	0.63
128	0.467	0.51	0.44	0.58	0.59
129	0.408	0.48	0.44	0.55	0.55
130	—	—	—	0.52	0.53
131	—	—	—	0.485	0.485
132	—	—	—	0.48	0.485

The calculated results of TKE distribution for ^{232}Th photofission fragments along with the experimental data are presented in Fig. 1. The deformation parameters for fission fragments with a mass number of more than 130 are as follows:

$$\beta_1 = \beta 2 = \begin{cases} 0.42 & \text{for } A < 135, \\ 0.45 & \text{for } A \geqslant 135. \end{cases} \tag{9}$$

The changes of deformation parameters for the fission fragments of ^{232}Th with a mass number of less than 130 ($A \leqslant 130$) are presented in Table I.

The calculated results of the total kinetic energy as a function of photofission fragments of ^{234}U along with the experimental data are presented in Fig. 2. The behavior of the changes of TKED for this nucleus are significantly different from other nuclei. This difference can be due to the influence of target thickness [16]. That is why this behavior is not seen

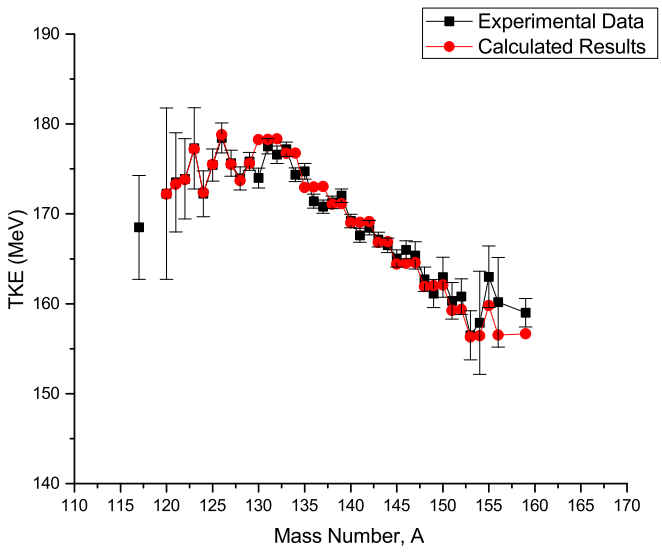

FIG. 2. Calculated total kinetic energy as a function of fragment mass at 6.8-MeV bremsstrahlung endpoint energy for photofission of ^{234}U along with the experimental data [15].

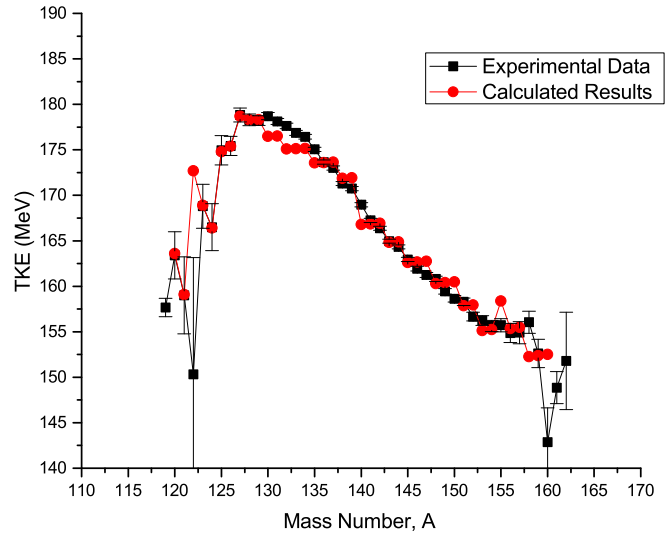

FIG. 3. Calculated total kinetic energy as a function of fragment mass at 6.5-MeV bremsstrahlung endpoint energy for photofission of ^{238}U along with the experimental data [15].

in other experimental data [15,42]. The deformation parameter for fission fragments with a mass number of more than 130 are as follows:

$$\beta_1 = \beta 2 = \begin{cases} 0.42 & \text{for } A < 135, \\ 0.45 & \text{for } 135 \leqslant A \leqslant 155, \\ 0.40 & \text{for } A \geqslant 155. \end{cases} \tag{10}$$

The changes of deformation parameters for the fission fragments of ^{234}U with a mass number of less than 130 ($A \leqslant 130$) are presented in Table I.

The calculated results of the TKE as a function of photofission fragments of ^{238}U along with the experimental data are presented in Fig. 3. The deformation parameters for fission fragments with a mass number of more than 130 are as follows:

$$\beta_1 = \beta 2 = \begin{cases} 0.45 & \text{for } A < 140, \\ 0.5 & \text{for } 140 \leqslant A \leqslant 155, \\ 0.45 & \text{for } A \geqslant 155. \end{cases} \tag{11}$$

The changes of deformation parameters for the fission fragments of ^{238}U with a mass number of less than 130 ($A \leqslant 130$) are presented in Table I.

The calculated results of the total kinetic energy as a function of photofission fragments of ^{240}Pu along with the experimental data are presented in Fig. 4. The deformation parameters for fission fragments with a mass number of more than 132 are as follows:

$$\beta_1 = \beta 2 = \begin{cases} 0.45 & \text{for } A < 140, \\ 0.5 & \text{for } A \geqslant 155. \end{cases} \tag{12}$$

The changes of deformation parameters for the fission fragments of ^{240}Pu with a mass number of less than 132 ($A \leqslant 132$) are presented in Table I.

The calculated results of the total kinetic energy as a function of photofission fragments of ^{242}Pu along with the experimental data are presented in Fig. 5. The deformation parameters for fission fragments with a mass number of more

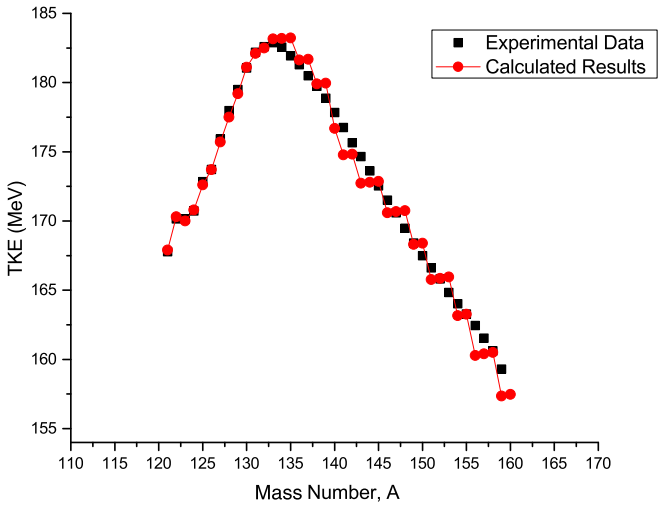

FIG. 4. Calculated total kinetic energy as a function of fragment mass at 20-MeV bremsstrahlung endpoint energy for photofission of ^{240}Pu along with the experimental data [17].

than 132 are as follows:

$$\beta_1 = \beta 2 = \begin{cases} 0.5 & \text{for } A < 143, \\ 0.55 & \text{for } A \geqslant 155. \end{cases} \quad (13)$$

The changes of deformation parameters for the fission fragments of ^{242}Pu with a mass number of less than 132 ($A \leqslant 132$) are presented in Table I.

As shown in Figs. 1–5, there is good agreement between the experimental and theoretical results of the uranium, thorium, and plutonium isotopes. Among these figures, the TKE distributions of plutonium isotopes are very smooth and orderly. This may be because the excitation energy of the experimental results of these isotopes (20 MeV) is more than the excitation energy of the experimental results of thorium and uranium isotopes, such as ^{235}U(n, f), which has a vibrational resonance of about 1.2-MeV excitation energy of the incident neutron [2]; the influence of the vibrational resonance may be slightly seen in the low-excitation energy of the results of thorium and uranium isotopes. Of course, this could also be due to the thorium anomaly [43,44].

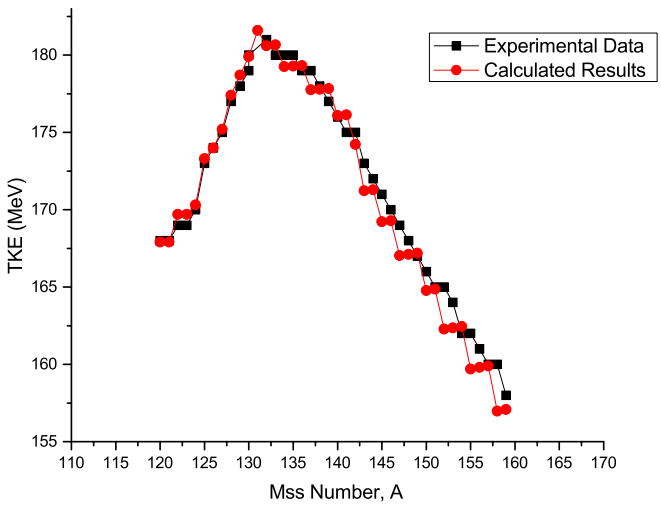

FIG. 5. Calculated total kinetic energy as a function of fragment mass at 20-MeV bremsstrahlung endpoint energy for photofission of ^{242}Pu along with the experimental data [17].

The deformation parameters for near symmetric fission fragments are presented in Table I. Table I indicates that there is good agreement between the calculated results and the experimental data, with a small variation in the deformation parameter except for a few fragments which have magic or semimagic neutron and proton numbers. As the mass number of the fissioning nucleus increases, the deformation parameters of the fission fragments with a greater mass number ($A \leqslant 132$) must change.

Here, because of the kind of calculations, the total fragment deformations ($\beta = \beta_1 + \beta_2$) are obtained at the scission point and the deformation of both fragments is assumed to be equal. So, the behavior of the TKED has been explained by the total fragment deformation at scission changes as in McGeorge *et al.* [24]. They concluded from the results of the Wilkins' calculations that the β values would increase at $Z = 50$ and 80. This could be explained as follows: Due to the presence (producing) of the magic nuclei (due to high binding energy), unstable complementary nuclei are formed, which have a huge change in the β parameter. For example, in the photofission of ^{240}Pu, according to Ref. [45], ^{117}Cd* is produced as a fission fragment that has a semimagic proton number. The complementary fragment of this fragment is ^{123}Ru. This complementary fragment has $N/Z \simeq 2$, which shows that it is a neutron-rich nucleus and therefore an unstable nucleus. On the other hand, while one of the fission fragments is a magic or semimagic nucleus ($N = 82$ or $Z = 50$), the other fission fragment is probably a rich neutron nucleus and an unstable nucleus. This effect greatly changes the β value in these nuclei. Pasca *et al.* [25,46] showed that the changing of deformation parameters for $A \leqslant 130$ in the model is more than for other deformation parameters. This is the region in which magic nuclei are more likely to form.

The deformation parameters change from $\beta_1 = \beta_2 \simeq 0.8$ for $A_H = 120$ to $\beta_1 = \beta_2 \simeq 0.5$ for $A_H = 130$. Specially, for the ^{232}Th nucleus, in the symmetrical region, there is a large increase in the values of the deformation parameters (unlike other fissioning nuclei); this increase maybe is due to the three humps potential, which is also seen in the shape of the mass distribution of the fission fragments.

In Table I, it is seen that the changes in deformation parameter values of fission fragments for the photofission of ^{242}Pu and for the photofission of ^{240}Pu are similar, while these values are significantly different for uranium nuclei (^{234}U and ^{238}U). This is due to the target thickness or the excitation energy ($\simeq$20 MeV) above the vibrational resonance range.

To predict the TKED of photofission, the experimental values of TKE distribution for spontaneous fission, neutron-induced fission, and photofission are investigated. First, the experimental values of the TKED for neutron-induced fission are examined and they are compared with photofission experimental values, and then the spontaneous fission is studied. By examining the experimental results of photofission and excitation energy, the TKE distribution for photofission of

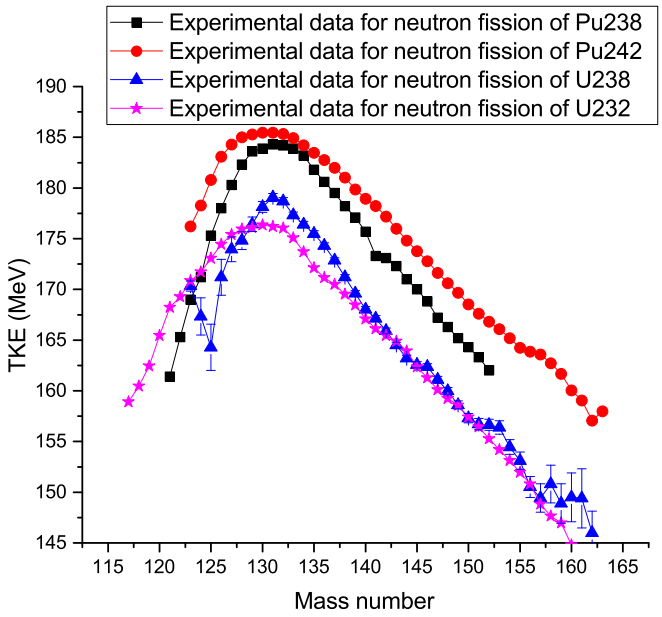

FIG. 6. The experimental values of total kinetic energy distribution for neutron-induced fission of ^{232}U [47], ^{238}U [2], ^{238}Pu [48], and ^{242}Pu [49].

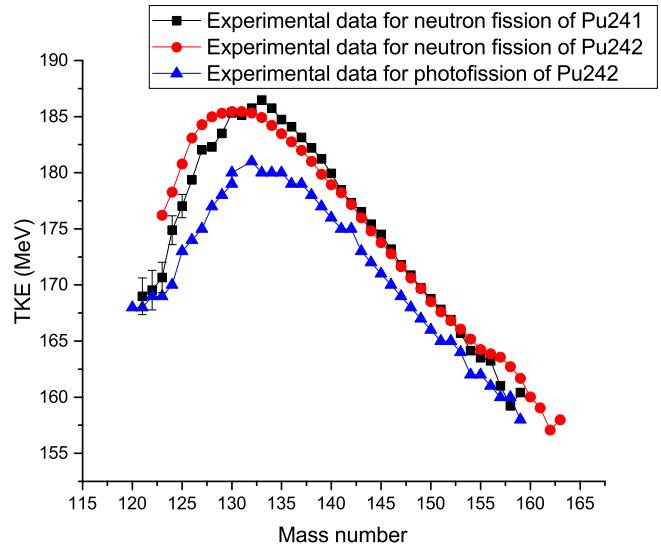

FIG. 7. The experimental values of total kinetic energy distribution for photofission of ^{242}Pu and neutron-induced fission of ^{241}Pu [50] and ^{242}Pu [49].

actinides is plotted. In Figs. 6–12, the experimental values of TKE distribution for spontaneous fission, neutron-induced fission, and photo fission are compared.

In Fig. 6 the experimental values of TKE for neutron-induced fission reactions on ^{232}U, ^{238}U, ^{238}Pu, and ^{242}Pu targets are compared. It is seen that the values of the TKE distribution for neutron-induced fission of ^{232}U and ^{238}U are closer together and also the TKE distribution values for neutron-induced fission of ^{238}Pu and ^{242}Pu are close together. But, generally, the TKE values observed for the fission fragments originated by the ^{238}Pu and ^{242}Pu targets are higher than the TKE values observed for the fission fragments originated by the ^{232}U and ^{238}U targets. This result is also seen when comparing the maximum TKE values of both fissioning nuclei ^{238}U and ^{238}Pu, which have the same mass number. They have the same behavior. Therefore, the TKE distributions of nuclei with the same mass number have a similar trend, but the maximum values of TKED for the same target nucleus occur in the fragments with the same mass number.

The experimental values of TKE distribution for neutron-induced fission of ^{241}Pu, ^{242}Pu, and photofission of ^{242}Pu are compared in Fig. 7. In this figure it is possible to observe that the TKE distribution values of fission fragments for the neutroninduced fission reactions on ^{241}Pu and ^{242}Pu targets are higher those those observed for the fission fragments produced by the photofission of ^{242}Pu. However, the excitation energy of neutron-induced fission of ^{241}Pu is lower (thermal induced) than the excitation energy of photofission of ^{242}Pu (20-MeV endpoint energy). Although the energy dependence of neutrons is about 8 MeV, the excitation energy difference is still considerable. Also, the TKE values of neutron-induced fission of ^{242}Pu and photofission of ^{242}Pu are different. So, the different reactions with the same compound nucleus have different TKE distributions. In Refs. [40,43] the mass distributions of photofission fragments are calculated by using the endpoint energy but the peak to valley ratios are calculated by using the average values of the excitation energy. While the average excitation energy for photofission of ^{242}Pu is 12.5 MeV and for neutron-induced fission of ^{241}Pu is 6.3 MeV [50], TKE values for neutron-induced fission of ^{241}Pu are higher than the TKE values for photofission of ^{242}Pu. Therefore, TKE values cannot be calculated correctly using either the endpoint energy or the average excitation energy.

Experimental values of TKE distribution for photofission and neutron-induced fission of ^{238}U and ^{232}Th are compared in Figs. 8(a) and 8(b), respectively. The behaviors of TKE distribution for photofission of ^{238}U and neutron-induced fission of ^{238}U show the same trend, but the mass numbers of fission fragments corresponding to the maxima TKE vary. The maximum value of TKE distribution for photofission of ^{238}U occurs for the mass number $A = 131$, whereas the maximum value for neutron-induced fission of ^{238}U occurs for mass numbers from $A = 127$ to $A = 130$. On the other hand, the TKE distributions for photofission and neutron-induced fission of ^{232}Th also show the same trend, but the their values for the mass numbers between 125 and 135 do not coincide for these two reactions. So, for uranium and thorium isotopes, unlike plutonium isotopes, the TKE values of photofission and neutron-induced fission are similar. This could be due to experimental results when the preneutron TKE distributions are presented for plutonium isotopes.

The experimental values of TKE distribution for photofission of ^{238}U and neutron-induced fission of ^{235}U and ^{237}Np are compared in Fig. 9. This figure shows that the TKE distributions for photofission of ^{238}U and neutron-induced fission of ^{235}U show the same trend, whereas the TKE values for fissioning nuclei with odd mass numbers are higher than the TKE values for fissioning nuclei with even mass numbers. Also, comparing Figs. 8 and 9, it can be seen that the TKE

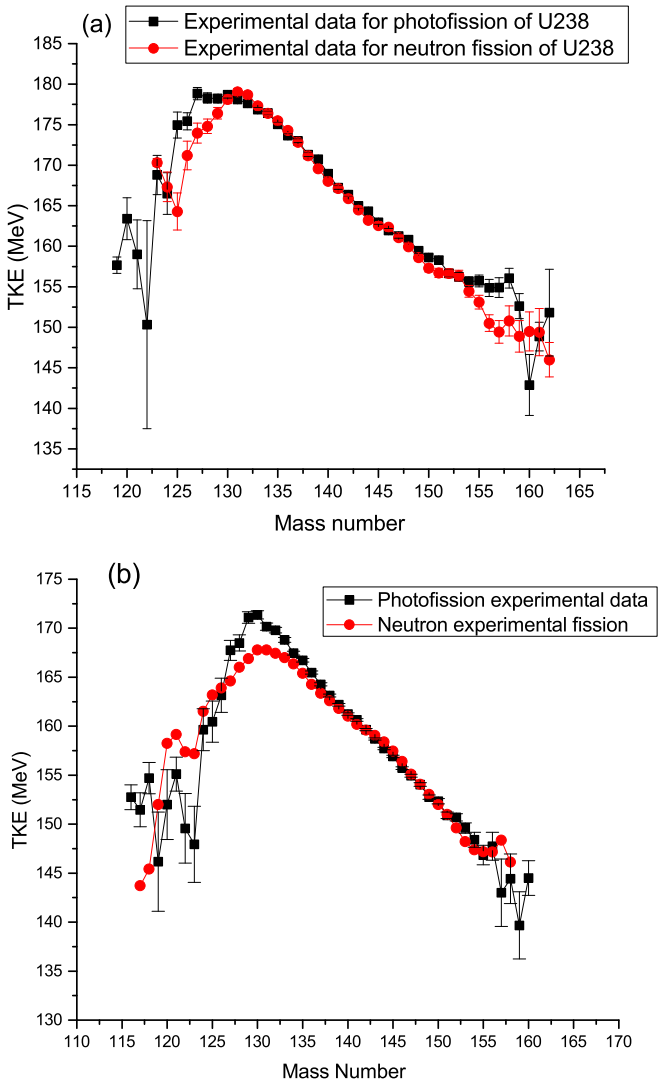

FIG. 8. The experimental values of total kinetic energy distribution for (a) photofission of ^{238}U [15] and neutron-induced fission of ^{238}U [2] and (b) photofission of ^{232}Th and neutron-induced fission of ^{232}Th.

distribution values for photofission of ^{238}U are closer to the TKE distribution values for neutron-induced fission of ^{235}U than to the TKE distribution values for neutron-induced fission of ^{238}U.

The experimental values of TKE distribution for neutron-induced fission of ^{235}U, ^{237}Np, ^{241}Am, and ^{239,241}Pu with odd mass numbers are compared in Fig. 10. This figure shows that the values of TKE distribution increase with increasing the mass number of the fissioning system. Also, the TKE distribution for neutron-induced fission of ^{235}U, ^{237}Np, and ^{241}Am shows the same trend, but the TKE distribution for neutron-induced fission of ^{239}Pu and ^{241}Pu decreases sharply near the symmetrical fission fragments. Because all nuclei do not have this rapid decrease in the symmetrical region, the odd number of neutrons or protons does not cause this phenomenon. So, this rapid decrease could be related to the formation of magic nuclei for the plutonium nucleus in this

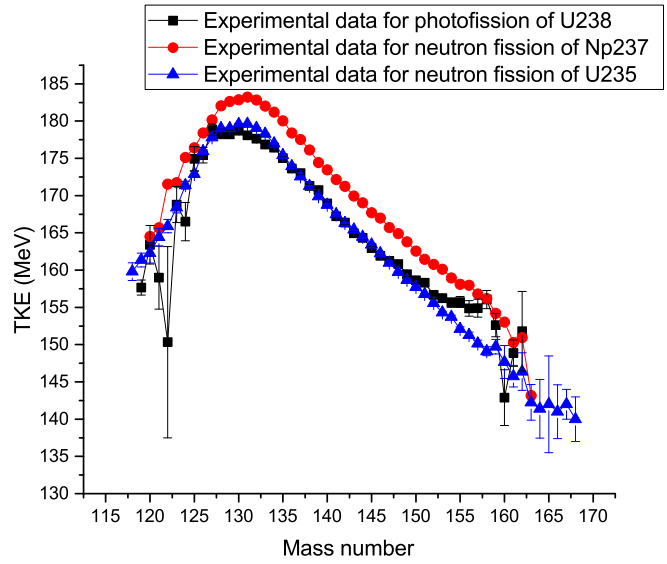

FIG. 9. The experimental values of total kinetic energy distribution for photofission of ^{238}U and for neutron-induced fission of ^{237}Np [51] and ^{235}U [52].

region. Also, there were differences between the results of the plutonium isotopes and other isotopes in Fig. 10 as can be seen in the previous figures. On the other hand, the experimental values of the neutron-induced fission of ^{239}Pu and ^{241}Pu are very close together.

Figure 11 represents a comparison made between the experimental values of TKE distribution for photofission and spontaneous fission of ^{238}U and ^{242}Pu. According to this figure, the values of TKE distribution for photofission and spontaneous fission are not the same. There is a difference between the TKE distributions for spontaneous fission and photofission concerning the slope as well as the maximum values. Therefore, the TKE distributions for spontaneous

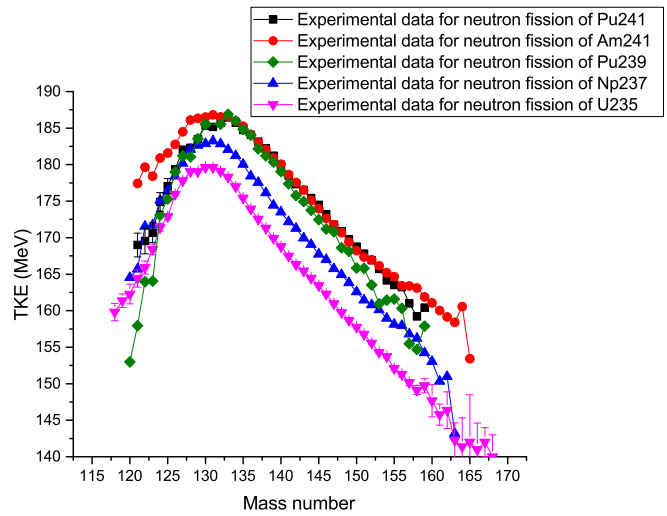

FIG. 10. The experimental values of total kinetic energy distribution for neutron-induced fission of ^{241}Pu [50], ^{241}Am [53], ^{239}Pu [54], ^{237}Np [51], and ^{235}U [52].

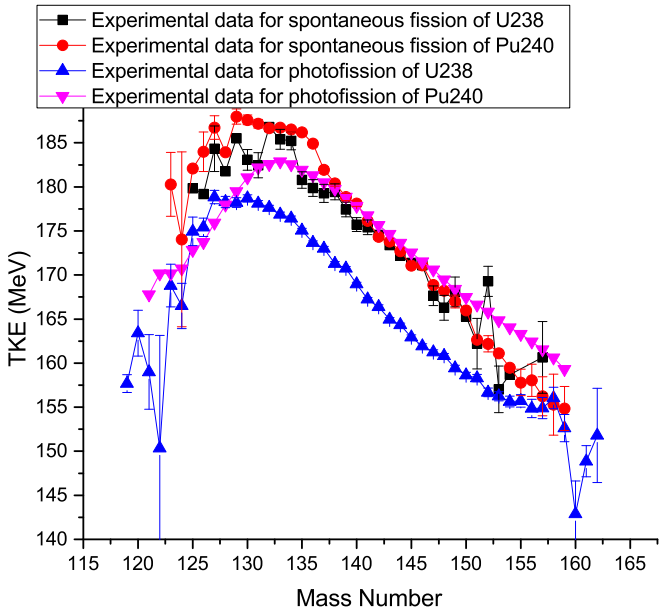

FIG. 11. The experimental values of total kinetic energy distribution for photofission of ^{240}Pu and ^{238}U and spontaneous fission of ^{240}Pu [23] and ^{238}U [23].

fission are not useful in evaluating the TKE values for photofission.

All available experimental values for TKE distribution of photofission are compared in Fig. 12. The behavior of TKED is similar for photofission of ^{232}Th, ^{238}U, and ^{240}Pu, while this not true for ^{234}U and ^{242}Pu. This behavior can be justified by the effect of target thickness in the case of ^{234}U photofission, as depicted in Fig. 2 [16]. An important point to note in Ref. [16] is that the target thickness is very effective on TKE results in the range of symmetrical fission

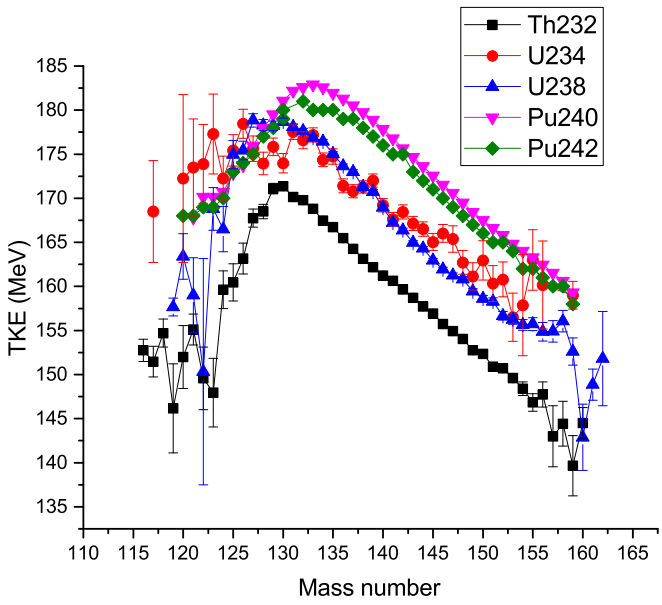

FIG. 12. The experimental data of total kinetic energy distribution for photofission of ^{232}Th, ^{234}U, ^{238}U, ^{240}Pu, and ^{242}Pu.

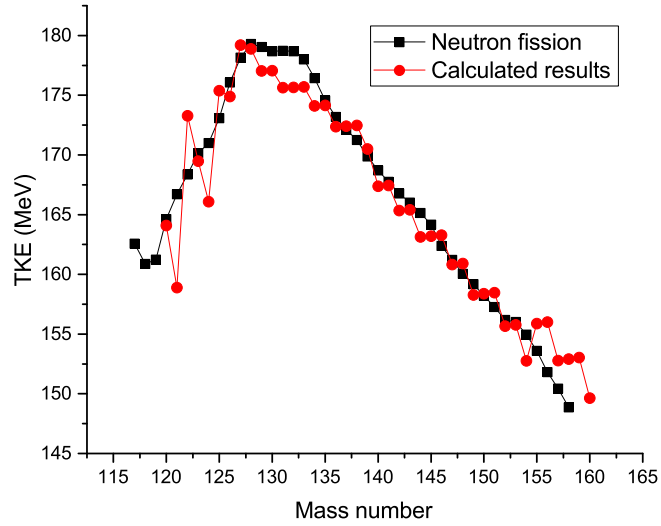

FIG. 13. Total kinetic energy distribution for photofission of ^{236}U in two ways: neutron-induced fission of ^{233}U (squares) and calculation values (circles) using the deformation parameters of ^{238}U photofission.

fragments. According to Ref. [16], for ^{234}U photofission, the change in symmetrical fission fragments relates to thin target thickness. Therefore, the symmetric mass region is not studied here. However, for the plutonium nucleus, the experimental values of the neutron-induced fission of ^{240}Pu and ^{242}Pu are very close together. These disturbances can also be seen for neutron-induced fission of ^{239}Pu and ^{241}Pu in Fig. 10. This may be due to the difference between the preneutron and postneutron TKE distribution or collective properties of plutonium isotopes, as discussed in Fig. 8. Therefore, as can be seen in Figs. 6 and 10, the TKE values for similar isotopes are closer results than the TKE values for other isotopes, and the TKE distributions of similar isotopes have a similar trend.

It is important to study the mean TKE changes by increasing excitation energy to represent the TKE distribution for other actinides. These changes are different for different reactions and nuclei. For example, according to Ref. [55], the average TKE increases up to about 10 MeV by increasing incident neutron energy up to 100 MeV. However, according to Refs. [2,56–58], the mean TKE for ^{234}U(γ, f) and ^{238}U(n, f) reactions increases by about 0.5 MeV by increasing 5 MeV of excitation energy. Therefore, the discussion is limited to incident neutron or γ energy of about 10 MeV.

As the mass number of fissioning nuclei increases, the maximum TKE distribution occurs in fission fragments with fewer mass numbers. Therefore, the TKE for photofission fragments of ^{236}U (circles) is calculated using the deformation parameters of ^{238}U photofission and is presented in Fig. 13. As can be seen in Fig. 9, the TKE distributions for neutron-induced fission of ^{235}U and for photofission of ^{238}U have a similar trend, so the TKED for neutron-induced fission of ^{233}U (squares) is presented in Fig. 13 along with the calculated results of TKED for photofission of ^{236}U. These two calculations are acceptably consistent, with only a natural difference in the symmetrical region.

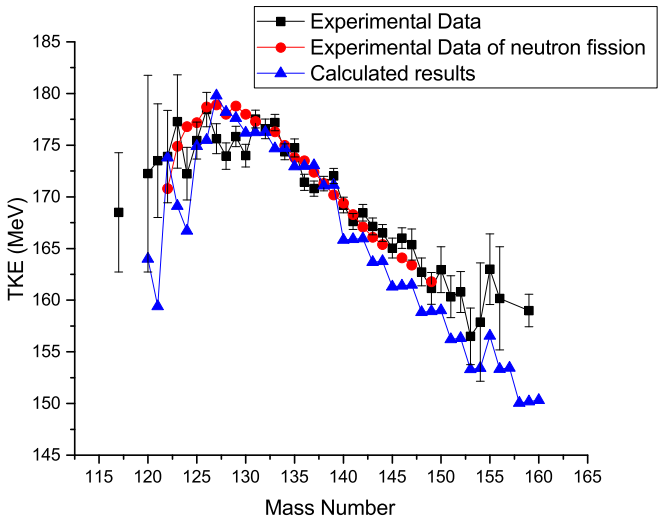

FIG. 14. Total kinetic energy distribution for photofission of ^{234}U: experimental values for photofission of ^{234}U (squares) [15], values for neutron-induced fission of ^{234}U (circles), and calculated results for photofission of ^{234}U (triangles).

Figure 14 represents the TKED calculations for photofission of ^{234}U. Experimental values for photofission of ^{234}U [15] are represented with squares and calculations for photofission of ^{234}U done using the parameters of photofission of ^{238}U are represented by triangles, along with the experimental values for neutron-induced fission of ^{234}U (circles). As can be seen, for fission fragments with a mass number greater than $A = 132$, there is a relationship between the TKE experimental values for neutron-induced fission and photofission of ^{234}U. However, calculations done using the deformation parameters of photofission of ^{238}U are not appropriate. So, the deformation parameters of photofission of ^{238}U were not used for uranium isotopes with a low-mass number. However, the sharp changes in the TKE experimental values for fission

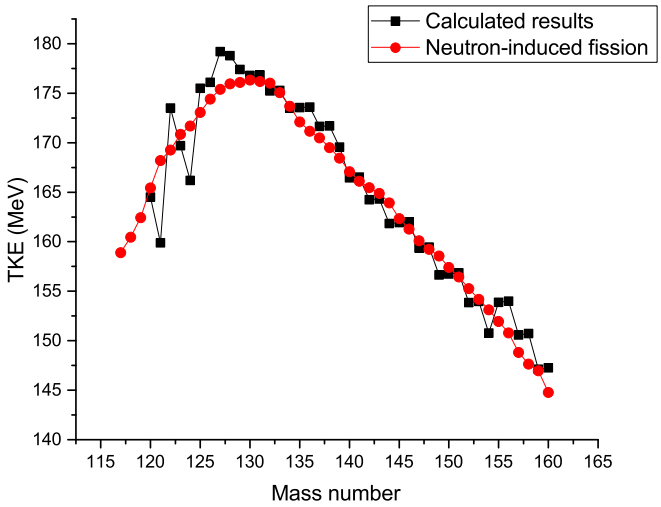

FIG. 15. Total kinetic energy distribution for photofission of ^{232}U: experimental values for neutron-induced fission of ^{232}U (circles) and calculated results for photofission of ^{232}U (squares).

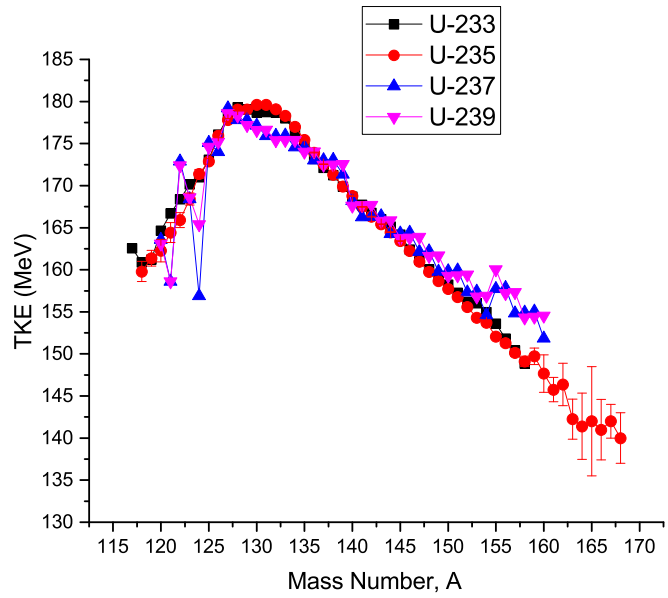

FIG. 16. Calculated total kinetic energy distribution for photofission of ^{233}U, ^{235}U, ^{237}U, and ^{239}U.

fragments with mass numbers of less than 132 are also seen in the experimental values for photofission of ^{234}U, due to the target thickness or resonance excitation energy (Fig. 12) [16].

Figure 15 represents the TKED calculations for photofission of ^{232}U. The results of ^{232}U photofission are calculated using the deformation parameters of ^{238}U photofission. Experimental values for neutron-induced fission of ^{232}U and calculated results for photofission of ^{232}U are in good agreement, as is shown in Fig. 8(a). The TKE values calculated with the deformation parameters for photofission of ^{234}U are higher than the experimental results of neutron-induced fission of ^{232}U, while these values are in good agreement with using the parameters of ^{238}U photofission. This difference can be due to

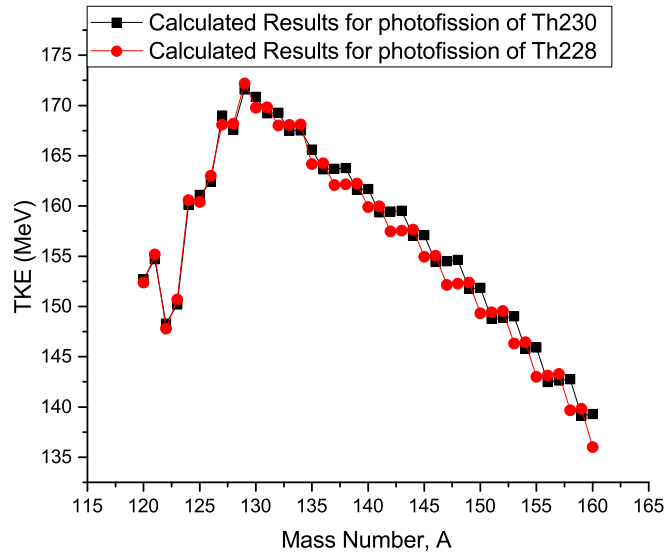

FIG. 17. Total kinetic energy distribution for photofission of ^{230}Th and ^{228}Th.

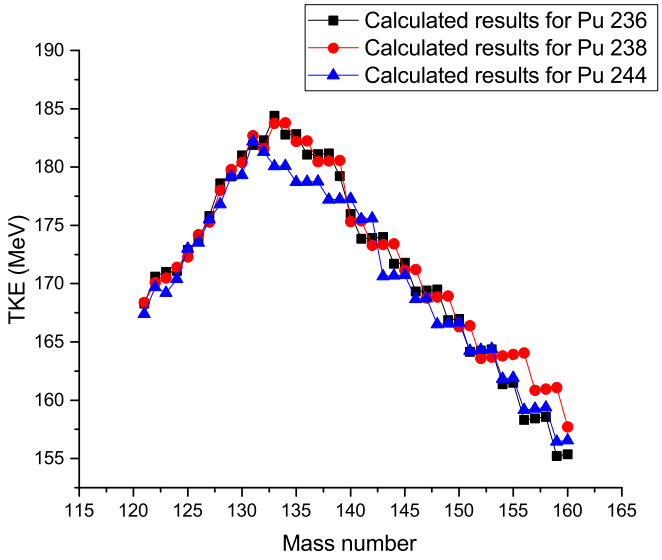

FIG. 18. Total kinetic energy distribution for photofission of ^{236}Pu, ^{238}Pu, and ^{244}Pu.

the experimental method that has made many changes in the experimental values (Fig. 12).

The TKE distributions for photofission of ^{233}U, ^{235}U, ^{237}U, and ^{239}U are represented in Fig. 16. Because there were no experimental results for odd-mass-number nuclei, TKE values for photofission of ^{233}U and ^{235}U are approximated with the experimental values of neutron-induced fission, and TKE values for photofission of ^{237}U and ^{239}U are calculated with quantification parameters of uranium-238 photofission calculations.

The TKE distribution for photofission of thorium isotopes with even mass numbers is evaluated using the parameters of ^{232}Th photofission within the scission point model, which is presented in Fig. 17. There are a few changes in TKE values of these two isotopes the same as for uranium isotopes in Fig. 16.

Also, the TKE distribution for photofission of plutonium isotopes with even mass numbers is presented in Fig. 18. The deformation parameters of fission fragments are selected the same as for photofission of ^{240}Pu to calculate the TKE values of photofission of ^{236}Pu and ^{238}Pu. The TKE values of photofission of ^{244}Pu are calculated using the deformation parameters of photofission fragments of ^{242}Pu. The TKE values slightly decrease with increasing the mass number of plutonium isotopes as seen for experimental data in Fig. 12.

IV. SUMMARY

The total kinetic energy distribution of photofission fragments was evaluated for uranium, thorium, and plutonium isotopes within the scission point model. There is good agreement between the experimental data and the theoretical results by fitting the deformation parameters of fission fragments. The results show that the deformation parameters of nuclei largely change in the magic-number fission fragments. Magic-number nuclei are usually formed with unstable complement components. The complement components have large deformation parameters that are clearly seen in model calculations.

The TKE distribution has also been investigated for neutron-induced fission, spontaneous fission, and photofission phenomena. It was found that TKE distribution depends on the mass and the atomic number of the compound nucleus and on the excitation energy. The compound nucleus with an odd mass number has more TKE values than the compound nucleus with an even mass number. The TKE distribution of even isotopes for photofission is almost the same as the fission of similar isotopes with three less mass numbers (odd nuclei). The TKE distribution of neutron-induced fission for thorium and uranium isotopes is similar to the TKE distribution for photofission of nucleus with the same mass and atomic number. However, the TKED of neutron-induced fission for plutonium isotopes does not have this property. This shows that the kinetic energy release in fission depends on the target nucleus and also indicates that TKE distributions for photofission and spontaneous fission are not similar.

Very little research has been done on the TKE distribution, especially for the photofission phenomena and odd nuclei, since there is no data on the TKE distribution for the photofission of odd-odd nucleus.

[1] F. J. Hambsch, H. H. Knitter, C. Budtz-Jorgensen, and J. P. Theobald, Nucl. Phys. A **491**, 56 (1989).
[2] F. Vives, F.-J. Hambsch, H. Bax, and S. Oberstedt, Nucl. Phys. A **662**, 63 (2000).
[3] J. P. Unik, J. E. Gindler, L. E. Glendenin, K. F. Flynn, A. Gorski, and R. K. Sjoblom, Phys. Chem. Fission **2**, 19 (1973).
[4] S. S. Kovalenko, K. A. Petrzhak, and V. M. Adamov, Sov. J. At. Energy **13**, 1092 (1963).
[5] D. L. Duke *et al.*, EPJ Web Conf. **146**, 04042 (2017).
[6] G. M. Ter-Akopian *et al.*, Phys. Rev. C **55**, 1146 (1997).
[7] U. Quade *et al.*, Nucl. Phys. A **487**, 1 (1988).
[8] W. Lang, H. G. Clerc, H. Wohlfarth, H. Schrader, and K. H. Schmidt, Nucl. Phys. A **345**, 34 (1980).
[9] L. Dematte, C. Wagemans, R. Barthelemy, P. Dhondt, and A. Deruytter, Nucl. Phys. A **617**, 331 (1997).
[10] R. Hentzschel, H. R. Faust, H. O. Denschlag, B. D. Wilkins, and J. Gindler, Nucl. Phys. A **571**, 427 (1994).
[11] C. Budtz-Jorgensen and H. H. Knitter, Nucl. Phys. A **490**, 307 (1988).
[12] G. Barreau *et al.*, Nucl. Phys. A **432**, 411 (1985).
[13] S. Pomme, E. Jacobs, M. Piessens, D. De Frenne, K. Persyn, K. Govaert, and M. L. Yoneama, Nucl. Phys. A **572**, 237 (1994).
[14] M. Piessens, E. Jacobs, S. Pomme, and D. De Frenne, Nucl. Phys. A **556**, 88 (1993).
[15] A. Göök, D. M. Chernykh, C. Eckardt, J. Enders, P. von Neumann-Cosel, A. Oberstedt, S. Oberstedt, and A. Richter, Nucl. Phys. A **851**, 1 (2011).

[16] A. Göök, C. Eckardt, J. Enders, M. Freudenberger, A. Oberstedt, and S. Oberstedt, Phys. Rev. C **96**, 044301 (2017).
[17] H. Thierens, A. De Clercq, E. Jacobs, D. De Frenne, P. D'hondt, P. De Gelder, and A. J. Deruytter, Phys. Rev. C **23**, 2104 (1981).
[18] B. A. Bochagov, A. P. Komar, and V. I. Fadeev, Sov. At. Energy **15**, 891 (1963).
[19] C. Schmitt *et al.*, Nucl. Phys. A **430**, 21 (1984).
[20] C. E. Bemis, Jr., Robert L. Ferguson, F. Plasil, R. J. Silva, F. Pleasonton, and R. L. Hahn, Phys. Rev. C **15**, 705 (1977).
[21] D. Hoffman, D. Lee, A. Ghiorso, M. Nurmia, and K. Aleklett, Phys. Rev. C **22**, 1581, (1980).
[22] E. A. Sokol, G. M. Ter-Akopyan, A. I. Krupman, V. P. Katkov, L. F. Nikonova, and N. V. Eremin, At. Energy **71**, 422 (1991); Sov. At. Energy **71**, 906 (1991).
[23] P. Schillebeeckx, C. Wagemans, A. J. Deruytter, and R. Barthelemy, Nucl. Phys. A **545**, 623 (1992).
[24] J. C. McGeorge *et al.*, Nucl. Phys. A **326**, 108 (1979).
[25] H. Pasca, A. V. Andreev, G. G. Adamian, and N. V. Antonenko, Eur. Phys. J. A **52**, 369 (2016).
[26] V. Manea and A. Tudora, Ann. Nucl. Energy **38**, 72 (2011).
[27] V. Yu. Denisov, T. O. Margitych, and I. Yu. Sedykh, Nucl. Phys. A **958**, 101 (2017).
[28] M. D. Usang, F. A. Ivanyuk, C. Ishizuka, and S. Chiba, Phys. Rev. C **96**, 064617 (2017).
[29] K. Pomorski, B. Nerlo-Pomorska, J. Bartel, and C. Schmitt, EPJ Web Conf. **169**, 00016 (2018).
[30] A. Ruben, H. Marten, and D. Seeliger, Z. Phys. A **338**, 67 (1991).
[31] F. A. Ivanyuk, S. Chiba, and Y. Aritomo, Phys. Rev. C **90**, 054607 (2014).
[32] F. Ivanyuk, T. Kawano, S. Chiba, M. W. Paris, and P. Talou, EPJ Web Conf. **122**, 01002 (2016).
[33] A. V. Andreev *et al.*, Eur. Phys. J. A **22**, 51 (2004).
[34] B. D. Wilkins, E. P. Steinberg, and R. R. Chasman, Phys. Rev. C **14**, 1832 (1976).
[35] C. Karthika, and M. Balasubramaniam, Eur. Phys. J. A **55**, 59 (2019).
[36] J. Blocki and W. J. Swiatecki, Ann. Phys. (NY) **132**, 53 (1981).
[37] J. Blocki, J. Randrup, W. J. Swiatecki, and C. F. Tsang, Ann. Phys. (NY) **105**, 427 (1977).
[38] X. Bao, H. Zhang, G. Royer, and J. Li, Nucl. Phys. A **906**, 1 (2013).
[39] N. Sugarman and A. Turkevich, in *Radiochemical Studies: The Fission Product*, edited by C. D. Coryell and N. Sugarman (McGraw-Hill, New York, 1951), Vol. 3, p. 1396.
[40] M. R. Pahlavani and P. Mehdipour, Nucl. Sci. Tech. **29**, 146 (2018).
[41] H. Umezawa, S. Baba, and H. Baba, Nucl. Phys. A **160**, 65 (1971).
[42] M. Verboven, E. Jacobs, M. Piessens, S. Pommé, D. De Frenne, and A. De Clercq, Phys. Rev. C **42**, 453 (1990).
[43] P. Mehdipour Kaldiani, Phys. At. Nucl. **82**, 450 (2019).
[44] H. Naik, A. Goswami, G. N. Kim, M. W. Lee, K. S. Kim, S. V. Suryanarayana, E. A. Kim, S. G. Shin, and M.-H. Cho, Phys. Rev. C **86**, 054607 (2012).
[45] H. Naik *et al.*, Nucl. Phys. A **853**, 1 (2011).
[46] H. Pasca, A. V. Andreev, G. G. Adamian, and N. V. Antonenko, Acta Phys. Pol., B **48**, 431 (2017).
[47] M. Asghar, F. Caitucoli, B. Leroux, P. Perrin, and G. Barreau, Nucl. Phys. A **368**, 328 (1981).
[48] M. Asghar, F. Caitucoli, B. Leroux, M. Maurel, P. Perrin, and G. Barreau, Nucl. Phys. A **368**, 319 (1981).
[49] V. G. Vorobyeva, N. D. Dyachenko, B. D. Kuzminov, A. I. Sergachev, and V. M. Surin, Conf. Neutron Phys. **3**, 270 (1973).
[50] H. Thierens, E. Jacobs, P. Dhondt, A. De Clercq, M. Piessens, and D. De Frenne, Phys. Rev. C **29**, 498 (1984).
[51] C. Wagemans, E. Allaert, F. Caitucoli, P. D'Hondt, G. Barreau, and P. Perrin, Nucl. Phys. A **369**, 1 (1981).
[52] S. Zeynalov, W. Furman, and F. J. Hambsch, Investigation of Mass-TKE Distributions of Fission Fragments from the 235U (n, f)-Reaction in Resonances, in *Proc. of the 13th ISINN Workshop* (2005).
[53] M. Asghar, F. Caïtucoli, P. Perrin, G. Barreau, and B. Leroux, Nucl. Phys. A **334**, 327 (1980).
[54] K. Nishio, Y. Nakagome, I. Kanno, and I. Kimura, J. Nucl. Sci. Technol. **32**, 404 (1995).
[55] R. Yanez, J. King, J. S. Barrett, W. Loveland, N. Fotiades, and H. Y. Lee, Nucl. Phys. A **970**, 65 (2018).
[56] A. Al-Adili, F.-J. Hambsch, S. Pomp, S. Oberstedt, and M. Vidali, Phys. Rev. C **93**, 034603 (2016).
[57] D. G. Madland, Nucl. Phys. A **772**, 113 (2006).
[58] D. L. Duke, Ph.D. thesis, Colorado School of Mines, Arthur Lakes Library, LA-UR-15-28829, 2015.